Temperature Effects on DC and RF Characteristics of 140 nm AlGaN/GaN HEMTs with Regrown Contacts

Biddut K. Sarker,[1] Nicholas P. Sepelak,[1] Dennis E. Walker Jr.,[2] Karen Nishimura,[1] Antonio Crespo,[2] Gary Hughes,[2] Andrew J. Green,[2] and Ahmad E. Islam[2]

[1]*KBR, Inc., Beavercreek, OH 45431 USA*
[2]*Air Force Research Laboratory, Sensors Directorate, Wright-Patterson AFB, Dayton, OH 45433, USA*
Emails: biddut.sarker.ctr@us.af.mil, ahmad.islam.2@us.af.mil

Keywords: RF, high temperature, T-gate, MSG, UPG, AlGaN/GaN HEMT.

Abstract

We conducted DC and small-signal RF characterization on AlGaN/GaN high-electron-mobility transistors (HEMTs) over a range of temperatures to examine temperature-dependent variations in key device performance metrics including transconductance (g_m), extrinsic cutoff frequency (f_T), maximum gain frequency (f_{max}), unilateral power gain (UPG), and maximum stable gain (MSG). Our findings indicate that device parameters decline with increasing temperature at a distinct rate. Specifically, a 100°C rise results in f_T and f_{max} dropping by about 8 GHz and 17 GHz, respectively, while MSG decreases by approximately 1 dB. These changes are inherent to the device physics and are not influenced by its geometry or operational mode.

INTRODUCTION

Wide bandgap (WBG) and ultra-wide bandgap (UWBG) semiconductors, along with thermally stable materials, are essential for electronics in high-temperature environments like hypersonic vehicles and spacecraft. Field-effect transistors using materials such as SiC, GaN, and β-Ga2O3 enable digital, RF, and power-switching devices to function reliably under extreme heat [1,2]. At the Air Force Research Laboratory (AFRL), we are advancing the high-temperature operation of GaN-based devices for RF applications [3-10]. Our previous studies were focused on temperature-dependent characterization of AlGaN/ GaN HEMTs made with 140 nm gate length (AFRL GaN140 technology [3] annealed ohmic source/drain (S/D) contacts. The temperature range for RF measurements was also limited to 175 °C because of instrument limitations. We have recently improved the HEMT technology by using regrown S/D contacts (AFRL GaN140+ technology) that offers lower contact resistance and better device scalability for improved device performance. We have also expanded the RF measurement capabilities to 300 °C. This article highlights our recent findings from DC and small-signal RF measurements of GaN140+ HEMTs from room temperature (RT) to 300°C.

DEVICE FABRICATION

HEMT devices were fabricated on 4″ 6H-SiC substrates having a Fe-doped GaN buffer, AlN+ $Al_{0.28}Ga_{0.72}N$ layer, and a GaN cap (Fig. 1). Mesa-isolated regions were created using photolithography and reactive ion etching. Ohmic contacts were defined using a channel mask, etched back and subsequently regrown. Ti/Al/Ni/Au metal contacts were deposited by e-beam in the S/D regions. The T-shaped gate contact of length L_g ~140 nm and a head width of ~750 nm was defined using e-beam lithography followed by Ni/Au metal deposition and lift-off. Additionally, a ~200 nm Si-rich SiN passivation layer was applied in the channel area. The devices were created with different source-drain spacings (L_{SD}) including 1 µm, 2 µm, and 3 µm.

DEVICE CHARACTERIZATION

We performed a comprehensive DC and RF characterization of devices measured across a 4″ wafer at room temperature and analyzed key device parameters. The statistical analysis of the DC device parameters is presented in Table I. The temperature-dependent device characterizations were performed using a MicroXact Probe Station integrated with a semiconductor parameter analyzer (Keysight B1500) and a vector network analyzer. WinCal and IVCAD software were used for RF calibration and data acquisition. To calibrate the system, the LRRM (Line-Reflect-Reflect-Match) calibration method was performed at RT using a standard ISS (impedance standard substrate). A sample die containing multiple devices was packaged on a Cu-shim and placed on a probe station chuck. The chamber was then pumped to reduce the pressure to approximately 0.1 Torr before raising the temperature on the thermal chuck. At each temperature, the system was allowed to settle for 15 mins before performing DC and RF (small signal s-parameters) measurements.

TABLE I
STATISTICS OF DIFFERENT PARAMETERS OF DEVICES FOR VARIOUS SOURCE-DRAIN SPACING (L_{SD}) ACROSS A 4″ GAN140+ WAFER.

Parameters	L_{SD} = 1 µm	L_{SD} = 2 µm	L_{SD} = 3 µm
R_{on} (ohm-mm)	1.11±0.06	1.38±0.09	1.70±0.11
I_{max} (mA/mm)	1428±69	1315±75	1268±73
I_{dss} (mA/mm)	1260±62	1158±64	1113±62
V_{th} (V)	-3.49±0.07	-3.45±0.07	-3.40±0.07
$g_{m,max}$ (mS/mm)	455±24	417±26	402±23

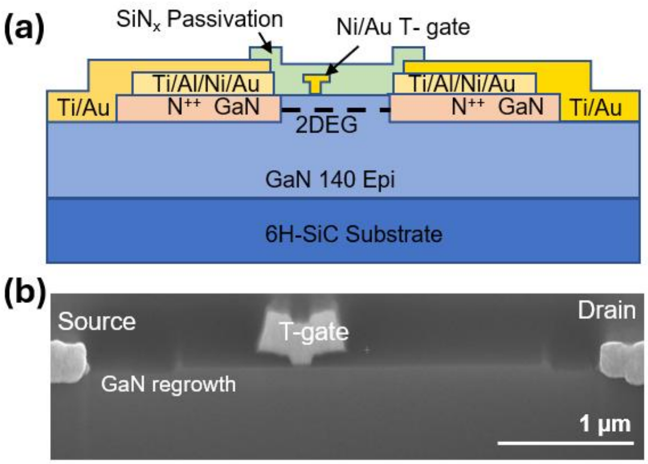

Fig. 1: (a) Schematic of typical AlGaN/GaN T-gate HEMT device under study. (b) A cross-sectional scanning electron microscope (SEM) image of an AlGaN/GaN T-gate HEMT device with a gate length (L_g) of approximately 140 nm, and a source-drain spacing (L_{SD}) of 3 µm. This SEM image was taken before the SiNx passivation process was applied to the device.

RESULTS AND DISCUSSION

Figures 2a and 2b show the drain current (I_{DS}) versus drain-to-source voltage (V_{DS}) characteristics of a HEMT device for various gate-to-source voltage (V_{GS}) from -4V to 0V at 25 °C and 300 °C, respectively. The output characteristics in Figure 2b indicate that the GaN devices experienced a 27% reduction in current carrying capacity when measured at V_{DS} = 10V and V_{GS} = 0V. This decrease is mainly due to lower carrier mobility and increased sheet resistance of the 2DEG layer as the temperature increases. To understand the reason behind the current reduction, we conducted tests on the transfer (I_D -V_{GS}) characteristics at different temperatures (Fig. 2c). Various DC device parameters such as transconductance, current on/off, leakage currents, threshold voltage, and on-resistance were calculated from the output and transfer curves. Variations in $g_{m,max}$, I_{max}/I_{min} and V_T were also examined as function of temperature (Fig. 2d - 2g). An 42% decrease in $g_{m,max}$ was observed due to enhanced phonon scattering at higher temperatures. Furthermore, a reduction in V_T was noticed because of increased off-state leakage caused by the flow of energetic carriers across the source-channel energy barrier [11, 12]. However, the off current at 300 °C is increased by approximately 100 times compare to that at 25 °C due to higher gate leakage from interdiffusion near the gate/barrier interface (Fig. 2c). We note that the GaN140+ (regrowth) platform does not demonstrate any significant improvements in high-temperature DC performance compared to the conventional GaN140 devices. However, it does offer substantial advantages due to a more robust manufacturing process. This includes precise control of source and drain spacing down to 1 µm, the elimination of alloy contamination, and enhanced RF performance due to improved scaling. These advancements

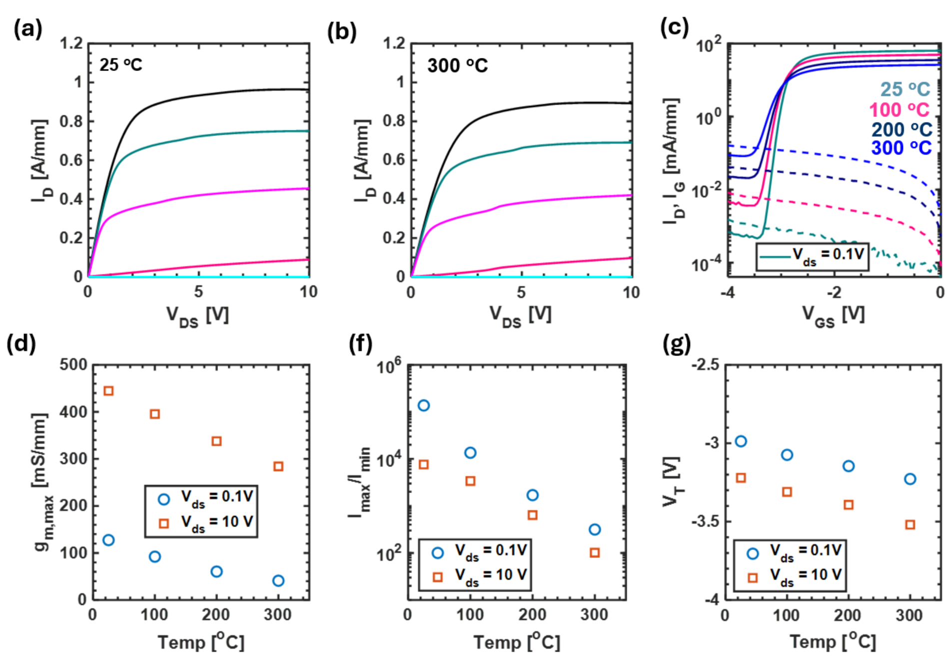

Fig. 2: Drain current (I_{DS}) versus drain-to-source voltage (V_{DS}) characteristics for various gate-to-source voltage (V_{GS}) from -4V to 0V in a vacuum at temperatures of (a) 25 °C, and (b) 300 °C. (c) Transfer (I_{Ds} -V_{GS}) characteristics of the same device under linear (V_{DS} = 0.1V) regime at various temperatures, ranging from 25 °C to 300 °C. The dashed lines represent the gate leakage currents. (d) Maximum transconductance ($g_{m,max}$) as a function of temperature. (f) Current on/off ratio as a function of temperature, and (g) Threshold voltage (V_T) as a function of temperature, measured in the linear (V_{DS} = 0.1V) and saturation (V_{DS} = 10V) regimes.

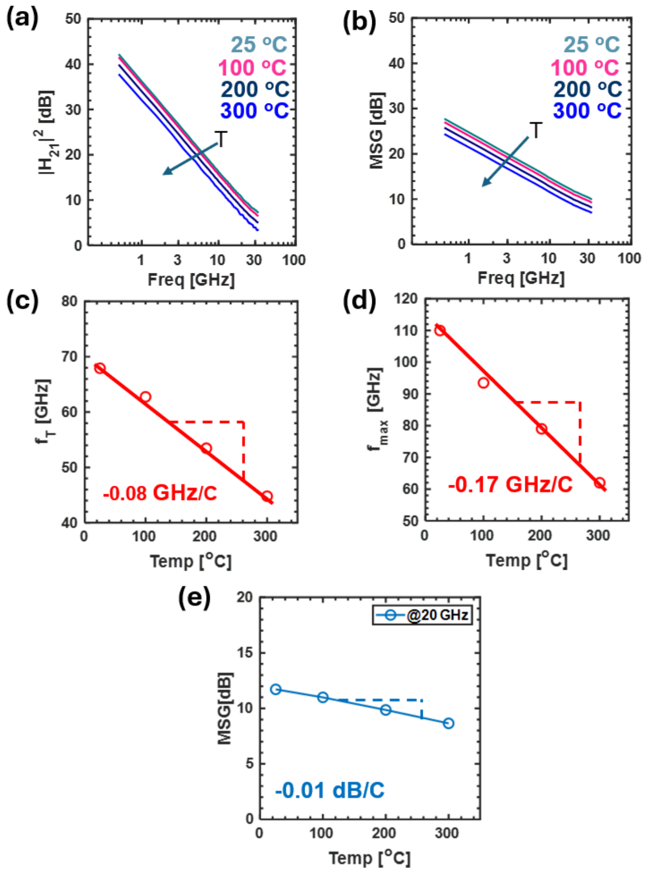

Fig. 3: (a) Variation of the H-parameter |*H21*|² versus frequency (*f*), (b) Variation of the *MSG* versus frequency (*f*) for a device at different temperatures *T* = 25, 100, 200, and 300°C. S-parameters were measured at the maximum of the saturation transconductance. The cut-off frequency (f_T) as a function of temperature was determined by finding the x-axis intercept of a -20 dB/dec line fitted to the |*H21*|² versus *log10(f)* characteristics. (c) Variation of f_T as a function of temperature. The slope of this curve is 0.08 GHz/°C. (c) Variation of f_{max} as a function of temperature. The slope of this curve is 0.17 GHz/°C. (e) Variation of MSG versus temperature. The slope of the 20 GHz curve is 0.01 dB/°C.

make the GaN140+ platform superior for high-frequency applications that require consistent manufacturing and precise dimensional control.

From the temperature-dependent small-signal S-parameter measurements, the various RF parameters such as H_{21} (Fig. 3a), MSG (Fig. 3b) and *UPG* values were calculated and plotted as frequency functions at different temperatures. Finally, the f_T, f_{max}, and *MSG* for various temperatures were extracted and plotted against temperature. It was observed that f_T (Fig. 3c), f_{max} (Fig. 3d), and MSG (Fig. 3e) all decrease as the temperature increases. Importantly, the rate of decrease for each parameter varies. An exciting discovery is that when the temperature is increased by 100°C, f_T, f_{max} and *MSG* decrease by 8 GHz, 17 GHz, and 1 dB, respectively.

Additionally, we investigated the temperature coefficients of various device parameters. The DC parameters, alongside the temperature-dependent RF parameters, were examined to understand their relationship. Furthermore, device physics and materials characterization were used to interpret the device performance at high temperatures. Temperature-induced variations in key device parameters were attributed to changes in electron transport (i.e., mobility, saturation velocity), and electrostatic control within the devices. Furthermore, material migration across interfaces was observed, contributing to performance degradation at elevated temperatures [3, 5]. Our analysis discovered that the variations in DC and RF performance with temperature are inherent to the device's physics, regardless of its geometry and mode of operation. This insight was gained by thoroughly analyzing the temperature-dependent intrinsic material properties of our GaN HEMTs and their correlation with temperature-dependent device performance.

We also examined device reliability by allowing devices to return to room temperature (RT) after high-temperature testing and conducting measurements. We found that the device characterization at RT remained nearly unchanged after the high-temperature testing. In addition, multiple measurements were performed on the same devices over several months and compared their performance. In these measurements, the testing parameters—including the bias conditions of the device such as, gate voltage, drain voltage, and the temperature range (25–300°C)—along with the measurement methodology, were maintained consistently as outlined in the previous section. Our findings showed that there were minimal changes (<5%) in RF parameters (such as f_T, f_{max}, and gain), indicating that the device transport remained stable over this period.

CONCLUSIONS

We conducted a temperature-dependent DC and small-signal RF characterization of AlGaN/GaN HEMTs at high temperatures. The results indicate that GaN140+ devices showed superior performance and reliability, with higher f_T and f_{max}, even at 300 °C. The RF performance metrics declined at a specific rate with increasing temperature. For every 100 °C increase, f_T, f_{max}, and *MSG* decreased by 8 GHz, 17 GHz, and 1 dB, respectively, over a temperature range from room temperature to 300 °C. The devices exhibited near-total recovery of their RF characteristics after being exposed to high temperatures and then returning to room temperature. This behavior provides valuable insights for optimizing GaN-based RF devices for reliable operation in extreme environments.

REFERENCES

[1] P. G. Neudeck, et. al. Proc. IEEE, vol. 90, pp. 1065-1076, 2002
[2] J. Watson et. al, J Mater Sci: Mater Electron, vol. 26, pp. 9226-9235, 2015
[3] A. E. Islam, et al, IEEE Trans. Electron Devices, 71 (3), pp. 1805-1811, 2024
[4] N. C. Miller, et al., IEEE J. Electron Devices Soc. 11, pp. 531-538, 2023
[5] A. E. Islam et al., IEEE Natl. Aerosp. Electron. Conf. (NAECON), Dayton, OH, pp. 263-268, 2023
[6] N. C. Miller, et al., IEEE J. Electron Devices Soc., vol. 11, pp. 531-538, 2023
[7] A. E. Islam et al., Appl. Phys. Lett., vol. 121, no. 24, p. 243501, 2022
[8] N. P. Sepelak et al., 2022 Compound Semiconductor Week (CSW), Ann Arbor, MI, pp. 1-2, 2022
[9] A. J. Green et al., IEEE Electron Device Letters, vol. 40, no. 7, pp. 1056-1059, 2019
[10] R. C. Fitch et al., IEEE Electron Device Letters, vol. 36, no. 10, pp. 1004-1007, 2015
[11] W. S. Tan, et. al., IEEE Electron Device Letters, vol. 27, no. 1, pp. 1-3, 2006
[12] S. Zhang, et. al., Appl. Phys. Lett., vol. 114, 013503, 2019

ACRONYMS

GaN: Gallium Nitride
AlGaN: Aluminum gallium nitride
HEMT: High Electron Mobility Transistor
2DEG: Two-Dimensional Electron Gas
UPG: Unilateral Power Gain
MSG: Maximum Stable Gain